Coding of position by simultaneously recorded sensory neurones in the cat dorsal root ganglion

R. B. Stein[1], D. J. Weber[1], Y. Aoyagi[1], A. Prochazka[1], J. B. M. Wagenaar[1], S. Shoham[2] and R. A. Normann[2]

[1]*Centre for Neuroscience and Department of Physiology, University of Alberta, Edmonton, Alberta, Canada*
[2]*Department of Bioengineering, University of Utah, Salt Lake City, UT, USA*

Muscle, cutaneous and joint afferents continuously signal information about the position and movement of individual joints. How does the nervous system extract more global information, for example about the position of the foot in space? To study this question we used microelectrode arrays to record impulses simultaneously from up to 100 discriminable nerve cells in the L6 and L7 dorsal root ganglia (DRG) of the anaesthetized cat. When the hindlimb was displaced passively with a random trajectory, the firing rate of the neurones could be predicted from a linear sum of positions and velocities in Cartesian (x, y), polar or joint angular coordinates. The process could also be reversed to predict the kinematics of the limb from the firing rates of the neurones with an accuracy of 1–2 cm. Predictions of position and velocity could be combined to give an improved fit to limb position. Decoders trained using random movements successfully predicted cyclic movements and movements in which the limb was displaced from a central point to various positions in the periphery. A small number of highly informative neurones (6–8) could account for over 80% of the variance in position and a similar result was obtained in a realistic limb model. In conclusion, this work illustrates how populations of sensory receptors may encode a sense of limb position and how the firing of even a small number of neurones can be used to decode the position of the limb in space.

(Received 24 May 2004; accepted after revision 25 August 2004; first published online 26 August 2004)
Corresponding author R. B. Stein: Centre for Neuroscience, University of Alberta, Edmonton, Alberta T6G 2S2, Canada. Email: richard.stein@ualberta.ca

Since Sherrington first described proprioception, investigators have tried to understand how a distributed population of sensory neurones throughout the body encodes posture and movement (Sherrington, 1906; Mountcastle, 1980; Bosco & Poppele, 2001; Gandevia *et al.* 2002). The proprioceptive sense of the angle of individual joints is derived from a multisensory integration of inputs from many receptors of differing types. Pulling on an isolated and externalized human tendon gives a sense of movement, implying that muscle receptors are involved in determining the angle of the joints that their muscles span (McCloskey *et al.* 1983). Anaesthetizing the skin and joints in humans reduces the accuracy of judgements about joint position, suggesting that these receptors are also involved in determining the position of individual joints (Gandevia *et al.* 1983; Collins *et al.* 2000; Gandevia *et al.* 2002). Finally, microstimulation of joint afferents and some cutaneous receptors evokes sensations of movement in human subjects (Macefield *et al.* 1990).

Most studies on the role of afferents in proprioception have examined the encoding properties of single receptors in isolation. In some studies, ensembles have been compiled from separate recordings, allowing correlations between firing rate and variables such as joint position and velocity or a muscle's length and force (Loeb *et al.* 1985; Prochazka & Gorassini, 1998*b*; Jones *et al.* 2001; Cordo *et al.* 2002; Ribot-Ciscar *et al.* 2003). The implicit assumption is that the central nervous system assembles the sensory activity into a useful representation of variables, such as joint angle, and the representation of each joint is eventually combined to give a sense of the position of our limbs with respect to the body. Since this representation may require a combination of many neurones, single-unit recording techniques are not adequate to study proprioception directly.

In this study we recorded simultaneously from populations of neurones in the L6 and L7 dorsal root ganglia (DRG) of anaesthetized cats. This enabled us to study directly how sensory information is encoded into the firing rates of a population of neurones and how these firing rates may be decoded to predict the position of the limb in space. Neural recordings were made while the hindlimb was passively moved through

 DOI: 10.1113/jphysiol.2004.068668

a variety of trajectories, including random, cyclical and centre-out paths. We used multivariate, linear regressions to model the relationship between hindlimb kinematics and sensory activity. The results demonstrate that limb trajectories can be accurately reconstructed from less than 10 selected neurones. The Appendix presents a model that demonstrates how even a few muscle receptors can provide accurate information about the end-point of a limb in a physiologically plausible way, without the need for complex trigonometric calculations from individual joint angles. The Discussion considers some methodological limitations, as well as the functional implications of our results for the normal sense of position.

Methods

The Animal Policy and Welfare Committee of the University of Alberta approved all procedures under the guidelines of the Canadian Council of Animal Care. Seven adult cats were anaesthetized with sodium pentobarbitone (40 mg kg^{-1} I.P.). A tracheal cannula was inserted to maintain respiration and a jugular catheter was used to administer fluids and the same anaesthetic, as required to maintain a surgical level of anaesthesia. The back was shaved and a skin incision was made along the mid-line of the back. Paraspinal muscles overlying the transverse processes of L5–S1 were removed and a laminectomy was performed to expose the spinal cord and dorsal roots. Two 5 × 10 arrays of penetrating microelectrodes (Cyberkinetics Inc., Foxborough, MA, USA) were implanted through the dura into the L6 and L7 dorsal root ganglia (DRGs) on one side with a high-velocity inserter (Rousche & Normann, 1992). Reference wires were placed in the fluid surrounding the DRGs and the skin flap was closed over the back. After surgery the animals were suspended in a spinal frame and radiant heat was used to maintain the body temperature near 37°C. At the end of the experiment the animal was killed using an overdose of the anaesthesia and the cessation of cardiac activity was monitored for several minutes.

Multichannel neural recording technique

The electrodes used in these experiments were arranged in a rectangular configuration with 5 rows of 10 electrodes, 1.5 mm in length and spaced 400 μm apart. In addition to providing many sites for recording action potentials, this dense arrangement of electrodes serves to anchor the implanted array among the densely packed cell bodies within the ganglion. The electrode arrays were connected to a 100- channel amplifier. The gain of the amplifiers was 5000 (bandwidth 250–7500 Hz) and signals from each electrode were sampled at 30 kHz. A Pentium class computer recorded and saved the signals in conjunction with a Neural Signal Acquisition System (NSAS; Cyberkinetics Inc.). This system required thresholds to be set on each channel and only saved brief (1 ms) segments of the signal around the time that the threshold was crossed (Guillory & Normann, 1999).

Single units were discriminated offline from the set of recorded waveforms on each electrode using a Matlab-based algorithm (Shoham *et al.* 2003). The waveforms were first projected onto their principle components (PC), and an expectation-maximization clustering algorithm then identified the number of clusters and their parameters (see Fig. 1).

Following the cluster estimation procedure, additional automated procedures for 'spike train editing' were applied (Stein & Weber, 2004). For example, an algorithm applied statistical tests to eliminate spikes that produced instantaneous firing rates more than double the smoothed firing rate and added spikes to long intervals that produced an instantaneous rate about half of the smoothed firing rate. These deviations occurred when an erroneous waveform was accepted or a correct waveform was missed; see Stein & Weber (2004) for a detailed justification. The spike-editing techniques facilitated analysis of units for which the threshold was not set ideally or the signal-to-noise ratio was marginal. For control purposes, we repeated the analysis using traditional analysis techniques. The results were virtually identical, but the variability was slightly greater with the unedited spike trains, as expected.

Sensory afferents were activated by palpation and manipulation of the hindlimb. The response properties were used to categorize each unit (Aoyagi *et al.* 2003). Briefly, the hip, knee, ankle and toes were moved manually to identify muscle and joint receptors. A hand-held vibrator (~140 Hz) was generally applied over the tendon or muscle belly to identify primary spindle afferents. Golgi tendon organs may have been missed, because the animals were deeply anaesthetized and the muscles were completely flaccid. Cutaneous receptors were identified by palpation (touch, pressure, pinch and vibration). Gentle blowing or focal touch was used to identify hair receptors. During each manipulation, 10 s recordings were made to document the waveform and response for each unit.

After the units on each electrode were categorized, various movements were applied to the foot manually or with a robotic manipulator. The manipulator had two DC servomotors (BE233DJ; Parker Hannifin, Rohnert Park, CA, USA) and was programmed to deliver repeatable movements. For example, to generate random movements, the manipulator moved through a series of positions selected at random from a rectangular grid of points in the sagittal plane and the velocity of each movement was also chosen at random over a range of speeds. The movements continued until all points in the grid had

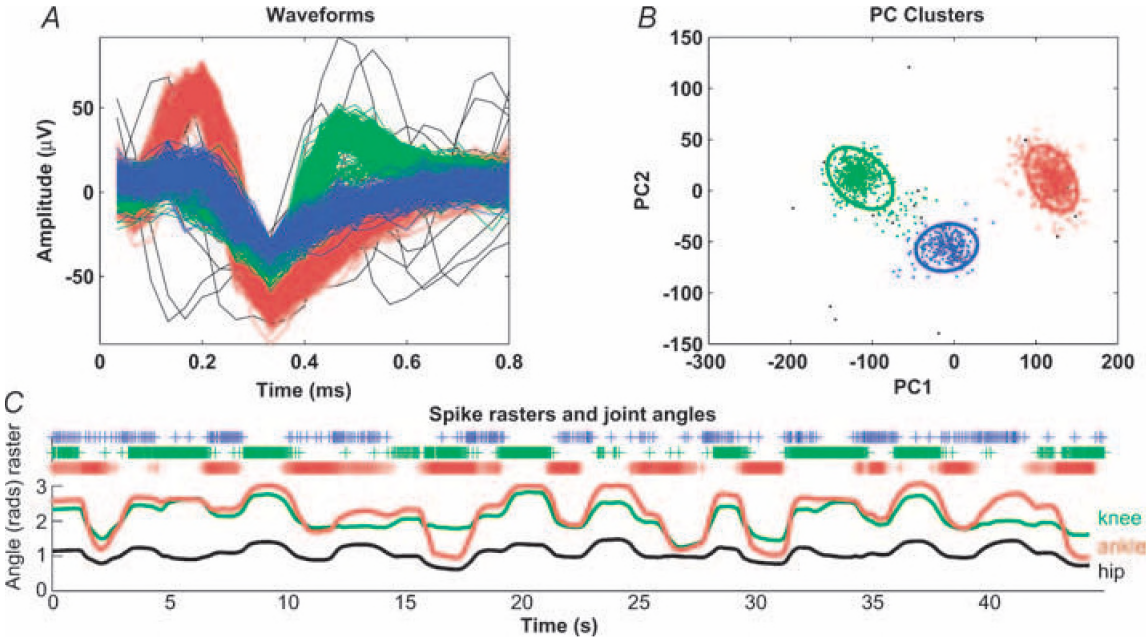

Figure 1. Methods for analyzing waveforms on a single electrode
Various waveforms recorded on one electrode were sorted (*A*) into three distinct units (red, blue and green) and unclassified waveforms (black) using cluster analysis in a space (*B*) representing the first two principal components (PC1, PC2) of the waveforms. The ellipses were computed using an automatic spike classifier (Shoham *et al.* 2003). The pattern of activity and joint angles are shown below (*C*).

been reached so there was a uniform coverage of the workspace. In several experiments, the identification and application of movements were repeated several hours later. For example, in one experiment in which 60 units were initially recorded 22 of them were still present in a second series of movements applied more than 4 h later. Thus, over a third of the units could be recorded for at least 4 h.

Kinematic recording technique

Walking-like, centre-out movements (from a central point to eight points in the periphery) and random movements were studied, all of which were largely confined to the sagittal plane. For example, the random movements (Fig. 2) covered most of the physiological range of the cat's hindlimb in the anterior–posterior plane (30 cm) and

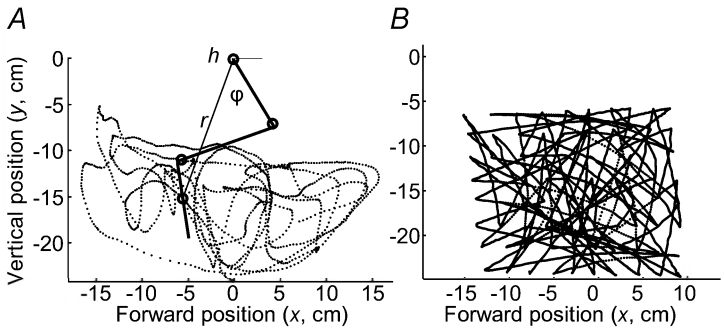

Figure 2. Methods for applying and recording movements
Position sensors (ϒ) were attached at the hip, near the knee and the ankle and on the paw near the metatarsophalangeal joint. From the positions of the sensors a stick figure of the cat's hindlimb in the sagittal plane was calculated. *A*, pseudorandom movement of the paw manually over its passive range of motion is shown as a dotted line. The position of the paw can be represented in terms of the forward (x) and vertical (y) position with respect to the hip (Cartesian coordinates). It can also be represented in polar coordinates as the distance (r) and the orientation angle (ϕ) of the paw with respect to the hip or in terms of the joint angles. Note that the orientation and hip (h) angles are measured with respect to the horizontal and increase as the hip and leg are extended. The knee and ankle angles (not shown) are defined according to the usual convention and increase with extension of the joint. *B*, random movements over a more restricted range (approximately 20 × 15 cm) using a robotic manipulator (see details in Methods).

in the vertical direction (20 cm), but only 1–2 cm in the medio-lateral plane. A U- shaped holder made of dental acrylic was fitted around the cat's paw, proximal to the metatarsophalangeal (MTP) joint. The top of the U was tied so that the paw was held securely. Any pressure on the skin was distributed widely and direct contact with the skin by the experimenters or the manipulator was minimized.

During manual movements of the limb, electromagnetic, motion-tracking sensors (6D- Research, Skill Technologies Inc., Phoenix, AZ, USA) measured the limb kinematics. Four magnetic sensors were placed on: (1) the skin near the hip joint; (2) the lateral epicondyle of the femur near the knee; (3) the lateral malleolus of the tibia near the ankle; and (4) the lateral surface of the foot holder near the metatarsophalangeal joint. For simplicity we will refer to this as the 'toe sensor' and use it as a measure of the toe position in space. To avoid skin slippage or displacement during movement, magnetic sensors (2) and (3) were rigidly fixed to the femur and tibia by surgical sutures through holes drilled in the respective bones. The distance of each sensor from its neighbouring joints was measured to allow calculation of the position of the joint centre. Intersegmental (joint) angles were calculated, together with the position of the toe sensor in rectangular and polar coordinates, using the hip sensor as the origin. The medio-lateral movements of the limb were also recorded, but were small (<2 cm) and are not shown. Results computed from the 3D angles, obtained with the electromagnetic motion-tracking system, were compared with those computed from 2D projections onto the sagittal plane and no significant differences in the fits were found. Therefore, 2D angles are analysed here.

The sampling rate of the 6D- Research system was 30 Hz and was well above the highest frequency components applied to the cat's paw (5–10 Hz). For the magnetic recordings we ensured that all instruments near the sensors, including sections of the spinal frame, contained no metal to avoid distorting the signals from the electromagnetic sensors. A synchronization pulse was used to align the neural and motion data offline.

A high-speed digital video camera (120 fields s^{-1}, GRDV9800R, JVC Corp.) recorded the limb movements produced by the robotic manipulator. A light-emitting diode (LED) was used to synchronize the video with the neural data. White markers were glued to the skin over the iliac crest, and the joint centres of the hip, knee, ankle and MTP joints. The centroid of the marker was automatically located in each image of the video using custom Matlab (Mathworks, Inc.) software. The camera plane was parallel to the sagittal plane of the leg. Calibration markers were spaced 10 cm apart in the horizontal and vertical planes and used to calibrate the camera view. Parallax errors were compensated by scaling the segment vectors by the measured separation distance between the ankle and MTP markers (i.e. foot length, which is constant).

Hip, knee and ankle joint angles were computed from the digitized marker positions, extension corresponding to a positive angular displacement. The knee marker was not used, because the skin overlying the knee tends to slide over the joint. Instead, the knee-joint angle was calculated using eqn (1), which follows from the law of cosines.

$$\theta_{\text{knee}} = \cos^{-1}\left(\frac{L^2_{\text{femur}} + L^2_{\text{shank}} - d^2}{2L_{\text{femur}}L_{\text{shank}}}\right), \qquad (1)$$

The three distances used in this calculation are: (1) L_{femur}, femur length; (2) L_{shank}, shank length; and (3) d, distance between the hip and ankle markers. The MTP was regarded as the end-point (toe position) for the limb measured in a polar coordinate system relative to the hip (r, radial distance; ϕ, orientation).

Neural encoding

A multivariate linear regression was used to model the firing rate of each neurone as a function of kinematic variables of the hindlimb (neural encoding). The full procedure included three processing steps.

(1) The neural and kinematic data were aligned at the LED onset time. Neural firing rates were calculated using the filter in eqn (2).

$$f_i = \frac{1}{\Delta t}\sum_j \left(1 - \frac{|t_i - t_j|}{\Delta t^2}\right). \qquad (2)$$

The firing rate (f_i) is computed at each time index i, t_i is the current time, t_j is the time of spike j in the interval $[t_i - \Delta t, t_i + \Delta t]$, and Δt is the sampling interval. Essentially, a contribution to the rate is added for the two nearest sample times for the kinematic variables in a way that all spikes are equally weighted and the mean time of the weights is the actual time of the spike. This method is similar to the partial binning methods previously described (Richmond *et al.* 1987; Schwartz, 1992; Stein *et al.* 2004).

(2) The rate function was filtered with a critically damped, second-order, low-pass filter (Stein *et al.* 2004). The impulse response of this filter is an EPSP-like waveform (Jack *et al.* 1975). Rate constants between 15 and 30 rad s^{-1} were used, corresponding to time constants of 67–33 ms. Different filters and other time constants for the EPSP-like filter were also applied using the Matlab function 'filt'. In general, longer time constants (more filtering) gave better fits, as expected. However, if the time constant was extended beyond the values cited, very little improvement was seen. The same filtering was also applied to the kinematic variables to avoid introducing relative time delays. Filtering was done after step (1) above to ensure that all spikes were given equal weight.

(3) The filtered firing rates were fitted to a weighted sum of position and velocity variables in each of three coordinate systems: Cartesian (x, y) and polar (r, ϕ) coordinates for the toe sensor, and joint angles (hip, knee and ankle) for the limb. This allowed a comparison of the predictions in Cartesian, polar and joint angular coordinates. For example, the predicted firing rate (g_i) for the i^{th} neurone can be written in Cartesian coordinates:

$$g_i = a_{i0} + a_{i1}x + a_{i2}y + a_{i3}\mathrm{d}x/\mathrm{d}t + a_{i4}\mathrm{d}y/\mathrm{d}t. \quad (3)$$

The five coefficients were chosen so as to minimize the difference between the predicted firing rates and the filtered firing rates for that neurone. If there are n neurones, the process was repeated for each neurone $(1 \leq i \leq n)$. Corresponding forms of eqn (3) were used to accommodate kinematics expressed in polar and joint angular coordinates. In joint coordinates, intersegmental angles (extension was taken as positive) were used to describe the limb position in the sagittal plane. In polar coordinates, the toe position and velocity were also expressed with respect to an origin at the hip, which was fixed in space. The variance accounted for (VAF) expressed as a percentage was used to evaluate the goodness of fit for each coordinate. Prediction of position in the sagittal plane requires combining coordinates and the root mean square (r.m.s.) error for the predictions was calculated. The coefficients of the linear encoding model (eqn (3)) describe the sensitivity of the neural response to each kinematic variable and linear correlation coefficients were also calculated for the relation between each kinematic variable and the firing rates.

Neural decoding

A linear filter model was used to reconstruct the hindlimb trajectories from the ensemble of neural firing rates f. Equation (4) shows the form of the model for decoding the horizontal (x) position of the toe in Cartesian coordinates:

$$\hat{x}_j = b_0 + b_1 f_{2,j} + \ldots + n_n f_{n,j} + bn + 1 f_{1,j-1} + b_{n+2} f_{2,j-1} + \ldots + b_{2n} f_{n,j-1}, \quad (4)$$

where $\hat{x}_j$ is the predicted value of x at the time point j. This is the prediction from the filtered firing rates of n neurones, based on the present (j) and one previous $(j–1)$ time point. In general, for L previous time points and n neurones, the decoding model takes the form:

$$\hat{x}_j = b_0 + \sum_{i=1}^{n}\sum_{k=0}^{L} b_{kn+i} f_{i,j-k}. \quad (5)$$

Similar, independent predictions were made for other variables, such as y, $\mathrm{d}x/\mathrm{d}t$ and $\mathrm{d}y/\mathrm{d}t$ in Cartesian coordinates and for variables in polar and joint angular coordinates. Values of L between 1 and 3 were used in the figures shown here. The b coefficients were chosen so as to minimize the mean square error between the predicted and measured values for each variable.

Equation (5) gives estimates of variables such as the x position and the velocity $\mathrm{d}x/\mathrm{d}t$. Integrating the velocity gives an independent estimate of the position. Using a weighted average of these two variables (eqn (6)) substantially improved the fit:

$$\tilde{x}_j = w(\tilde{x}_{j-1} + \mathrm{d}\hat{x}_j/\mathrm{d}t\Delta t) + (1 - w)\hat{x}_j, \quad (6)$$

where $\tilde{x}_j$ is the new estimate using a weight of w. To start the process, $\tilde{x}_0 = x_0$. The weight w was varied between 0 and 1 to find the best estimate of $\tilde{x}$. Note that for $w = 0$, only position information is used and for $w = 1$, only velocity information is used, except for the initial condition. Predictions were made for the other variables in each of the coordinate systems. Although eqn (6) is somewhat *ad hoc*, eqn (7) and the Appendix describe a related method for combining velocity and position information, based on the properties of muscle spindles, which respond to both length and velocity. Decoding with a leaky integrator (eqn (8)) having properties close to those found for muscle spindles gave equally good fits.

Results

Seven animals were studied, in which arrays of 50 electrodes each were implanted in the L6 and L7 DRGs. Four hundred and nineteen units were identified in terms of their receptive fields. The total numbers identified in each experiment were: 73, 24, 48, 90, 61, 81 and 42. Of the total, 53% were muscle receptors and 47% were from other sources (skin, hair, joints, etc.; see also Aoyagi *et al.* 2003). Forty-nine per cent were recorded from the L6 dorsal root and 51% from the L7 root. Additional units were discriminated (see Methods), but were not individually identified as to their receptive field or type. For example, in the fourth animal a total of 140 units were discriminated from 59 channels and in the fifth 87 units from 37 channels. Thus, nearly half the electrodes in these experiments recorded single units and each recorded 2.4 units on average.

Figure 2*A* shows the path of the paw as it was moved pseudorandomly (dotted line). The movements were applied manually and covered most of the passive range of motion (about 15 cm forward, backward and upward). In Fig. 2*B* a robot applied movements as a series of point-to-point movements over a more restricted grid of points in the sagittal plane; see Methods and Stein *et al.* (2004). Firing rates were computed at the sampling times for the kinematics (see Methods). The response surface maps in Fig. 3 illustrate firing rates as a function of limb position (x, y) for the movements of Fig. 2*A*. Figure 3*A* shows the firing rate of a slowly adapting cutaneous afferent with a receptive field on the front of the knee

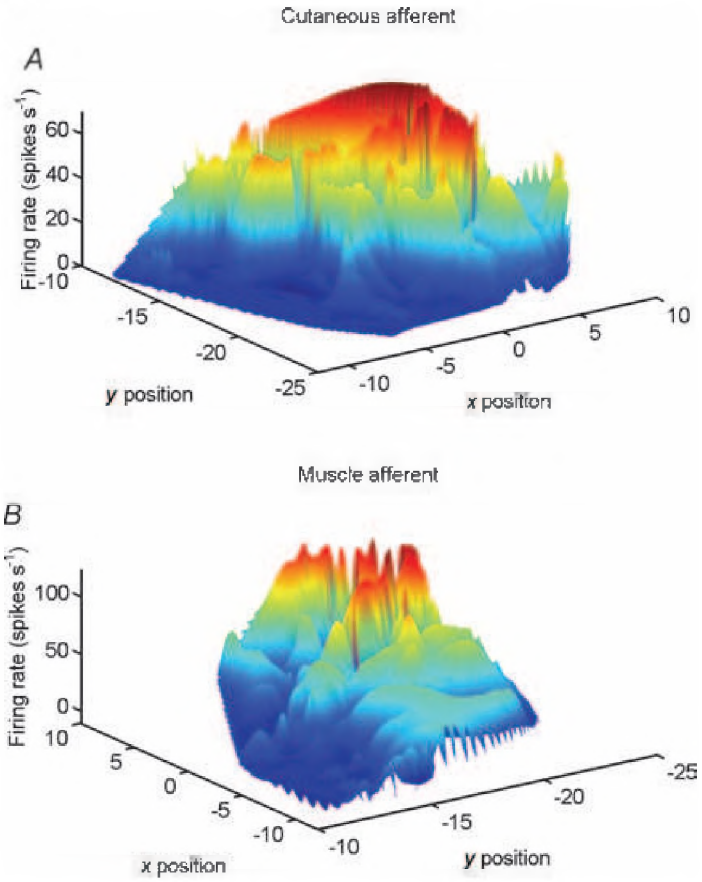

Figure 3. Surface plots for cutaneous (*A*) and muscle afferents (*B*) showing the variation in firing rate (vertical axis) as the toe is moved throughout the sagittal plane (*x* and *y* positions in cm)
The bin width was 0.5 cm and a 2D moving average filter with 5 bins was used to smooth the data. Note that the perspectives are different in the two parts of the figure, so that the peak firing rates are at the back and do not obscure other data.

(trends are highlighted by colour-coding). When the toe was raised, for example from 20 to 15 cm below the hip, its firing rate increased because the skin around the knee was stretched. Similarly, it fired faster when the toe was moved forward. Figure 3*B* shows the firing rate of a hamstring muscle spindle afferent that responded to knee extension and hip flexion. These movements were correlated with downward and forward movements of the toe. Thus, the firing rate of single sensory neurones can be correlated with movement of the toe with respect to the hip.

The first question pursued in these experiments was to what extent is the firing rate correlated with various kinematic variables? We addressed this question by testing the predictive power of the encoding model (using the 50 cells that showed the best correlations in a given trial). As shown in Fig. 4, about 30% of the variance in firing rate was related to the x and y position of the limb as defined in Fig. 2. Velocity accounted for about 20% of the variance, but acceleration accounted for less than 5%. Furthermore, combining position and velocity (the 4th set of bars in Fig. 4) accounted for a percentage of variance that approached the sum of the values for each variable alone (the 1st and 2nd set of bars). Since the firing can be described in terms of positions and velocities, the amplitudes and preferred directions can be calculated from the coefficients in the encoding models for both position and velocity. For example, from eqn (1) the amplitude A in position space for the i^{th} neurone is $A = \sqrt{(a_{i1}^2 + a_{i2}^2)}$ and the direction is $\alpha = \tan^{-1}(a_{i2}/a_{i1})$. Figure 5 shows the distributions in one data set of all cells for which the VAF was more than 40%. There are a wide range of amplitudes and preferred directions.

These kinematic variables accounted for nearly half the variance in Cartesian (x, y) coordinates (Fig. 4). The fit was somewhat better in polar coordinates and joint

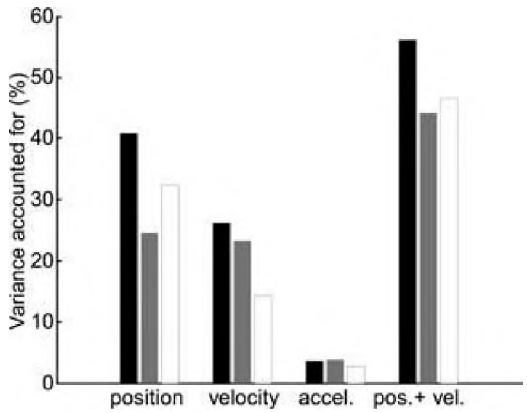

Figure 4. The average VAF (%) in the firing rate of the 50 cells most closely correlated with the kinematic variables
Three different random data sets are shown from three experiments. The largest contributions are from position and velocity and their contributions approximately sum.

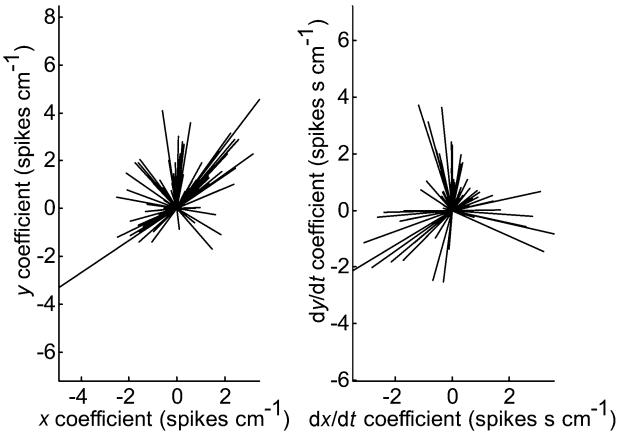

Figure 5. Preferred directions in position and velocity space are given by the coefficients from the encoding model using coefficients in Cartesian coordinates from a random data set
All illustrated units had a VAF > 40%. Note the wide range of preferred directions for both the position (left panel) and the velocity (right panel) coefficients.

angular coordinates (Aoyagi *et al.* 2003; Stein *et al.* 2004). Figure 6 shows the firing rates of 4 neurones fitted to the kinematics in joint angular coordinates. The units were: the best fitting neurone (Fig. 4*A*); the 3rd best (Fig. 4*B*); the 10th best (Fig. 4*C*); and the 30th best (Fig. 4*D*). Clearly, the major features that generate firing in these sensory cells are captured, although the details are progressively less accurate as VAF declines from Fig. 6*A* to *D*.

Sensory decoding

In contrast to the *encoding* of kinematic information in the firing rates of neurones, *decoding* involves the prediction of limb position from the firing patterns of a population of neurones. Various decoding methods have been proposed (Bialek *et al.* 1991; Salinas & Abbott, 1994; Schwartz, 1994; Wessberg *et al.* 2000; Scott *et al.* 2001; Serruya *et al.* 2002; Taylor *et al.* 2002), and we have chosen a linear filter similar to Wessberg *et al.* (2000) and Serruya *et al.* (2002). Figure 7 illustrates the results of decoding toe position in polar coordinates from the firing rates of 30 neurones. Polar coordinates were used since they gave rather better predictions than Cartesian coordinates. Firing rates and kinematic data (positions and velocities) from the first half of a trial were used to identify the coefficients of the model (training set). Data from the second half of the trial were used to test the model's ability to predict toe position (test set). Figure 7*A* illustrates the fit of the model to the training set. The VAF (training) was 99 and 98% for the distance and orientation variables, respectively, in polar coordinates using 30 units in the calculation. The root mean square (r.m.s.) errors were a few millimetres and <0.1 rad, respectively, so the actual (continuous lines) and predicted (dots) positions superimpose for the most part. From these values the x and y position of the paw could be calculated to an accuracy of about 1 cm. Figure 7*B* demonstrates the ability of the model to predict movements for the second half of the data (test set). The VAF was reduced (82 and 93%, respectively) and the accuracy in prediction was correspondingly poorer. The test predictions used the 5 neurones with the best correlation to the kinematic variables.

Figure 8 illustrates the effect of the number of neurones on the training and test performance. For this analysis the neurones were rank-ordered by their encoding correlation coefficients in the training set. One to fifteen neurones were selected according to their rank (highest first).

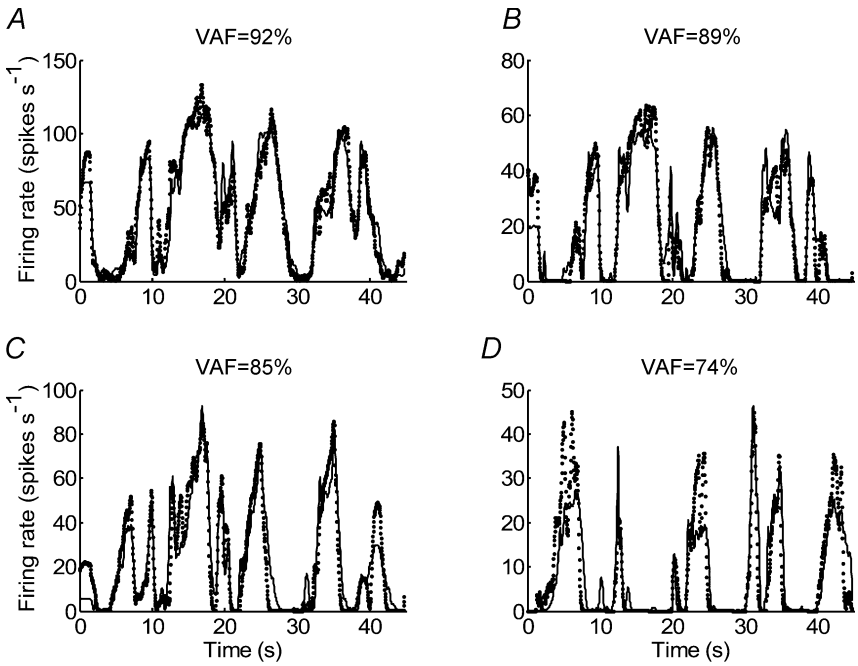

Figure 6. Comparison of the actual (line) and predicted firing rates (dots) for the best fitting (*A*) the 3rd best (*B*), the 10th best (*C*) and the 30th best fitting neurone (*D*)
The VAF (%) is shown for each unit.

These same neurones were then used to predict the movement in both the training and the test sets. As the number of neurones in the training set increased, the predictions became monotonically better. The VAF with 50 neurones was nearly 100% and the r.m.s. error was ~1 cm. Predictions using only the one neurone, whose firing was best correlated to each kinematic variable, accounted for about 70% of the variance in position in both the training and the test sets in the two experiments shown. Interestingly, the best neurones for both r and ϕ in the two experiments were muscle receptors from the hip and knee (see Table 1). In the test set, as more neurones were added, the VAF increased and reached a plateau between 80 and 90% with 6–8 neurones. The VAF actually began to decline when more poorly correlated neurones were added. Similarly, the r.m.s. error decreased up to a point and then began to increase as more neurones were added. The r.m.s. error provides information related to, but not identical to the VAF. For example, if the predicted data were offset from the actual positions by 1 cm, but followed the variations in limb position perfectly, the VAF would be 100%, but the r.m.s. error would be 1 cm.

Table 1 gives the identified neurones with the best correlation to each kinematic variable for data sets in two experiments. These units were predominantly muscle receptors (30/40; 75%) from the L6 ganglion (27/40; 68%), often from bi-articular muscles (12/30; 40%). The values are higher than the overall percentages given at the beginning of the Results (53% muscle and 49% L6) and in our recent publication; 30% biarticular muscles (Aoyagi *et al.* 2003). This suggests that muscle receptors, particularly from proximal bi-articular muscles are particularly useful in predicting overall limb position. For example, the posterior portion of biceps femoris stretches from near the hip to near the ankle in the cat. The firing of a muscle receptor in this muscle should therefore be well correlated with the distance from the hip to the end-point. In contrast, a receptor in gastrocnemius will mainly signal ankle and to a lesser extent knee position, but will not be so correlated to a global variable. However, even receptors in the toes can give information about limb

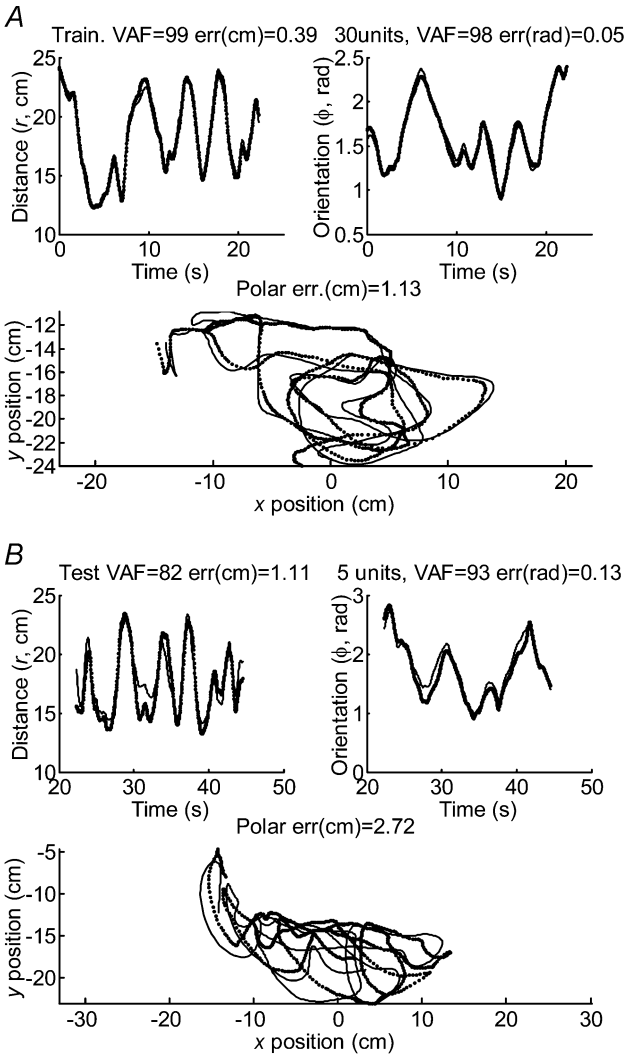

Figure 7. Predicting position in training (*A*) and test (*B*) sets
A, decoding position using 30 neurones (training) in polar coordinates (distance r and orientation ϕ) for the first half of a data set. From the polar coordinates the x and y coordinates were calculated. The VAF (%) and r.m.s. error are shown for each variable. *B*, decoding results for the second half of the data set (test) using the 5 best neurones identified in the training set. Actual (continuous lines) and predicted positions (dots) are shown in each part.

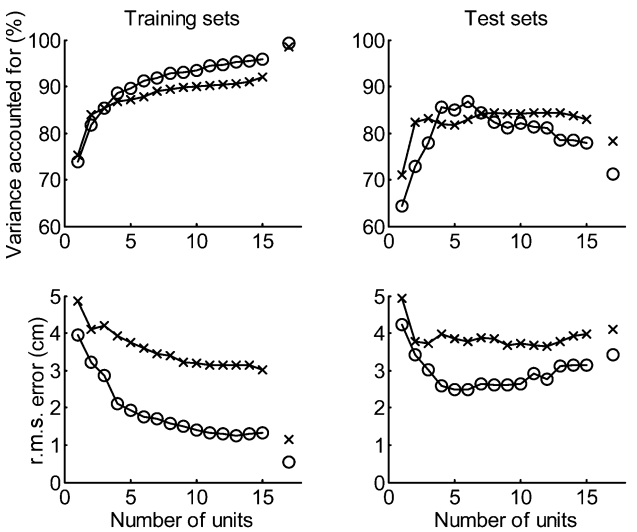

Figure 8. Increasing the number of units used to fit the first half of a data set (training) increases the VAF and decreases the r.m.s. error
When applying the parameters from the training set to the second half of the data set (test), the VAF generally reaches a peak and the r.m.s. error a minimum with 5–10 neurones. Data are shown from two different experiments. The values for 50 neurones are shown at the far right of the graphs (x, o).

Table 1. Receptive fields of the 5 units that showed the best absolute correlations to each of the kinematic variables studied in polar coordinates (r, ϕ, dr and dϕ)

	Exp. 1				Exp. 2					
	Corr. coef.	Unit	Root	Type	Loc./resp.	Corr. coef.	Unit	Root	Type	Loc./resp.
r	0.6532	56.2	L6	mus.	hf	0.7499	70.3	L6	mus.	he/kf
	0.6432	74.2	L6	mus.	ke	0.6311	55.1	L6	mus.	kf
	0.6205	87.3	L6	mus.	kf/he	0.6168	13.1	L7	mus.	ae
	0.6085	56.3	L6	cut.	med. leg	0.4296	68.1	L6	cut.	toe pad
	0.5433	65.1	L6	mus.	kf/he	0.3466	33.1	L7	mus.	te
ϕ	0.6222	79.2	L6	mus.	kf/he	0.6579	63.1	L6	mus.	hf
	0.5515	98.1	L6	mus.	hf/ke	0.637	14.1	L7	mus.	af
	0.5511	16.2	L7	mus.	ke	0.6321	43.1	L7	cut.	ant. leg
	0.5439	52.3	L6	mus.	hf	0.627	68.1	L6	cut.	toe pad
	0.5097	89.2	L6	mus.	he/kf	0.6074	13.1	L7	mus.	AE
dr	0.6305	5.1	L7	mus.	ae	0.6937	13.2	L7	mus.	af
	0.5654	87.3	L6	mus.	kf/he	0.6878	32.2	L7	cut.	lat. leg
	0.5569	66.1	L6	mus.	kf/he	0.6708	43.1	L7	cut.	ant. leg
	0.5318	54.3	L6	mus.	ae	0.6692	25.1	L7	joint?	toe
	0.5288	68.3	L6	cut.	med. a	0.6414	86.2	L6	cut.	vib. foot
dϕ	0.7602	100.1	L6	mus.	hf	0.6192	70.3	L6	mus.	he/kf
	0.6888	83.1	L6	cut.	foot	0.4817	13.1	L7	mus.	ae
	0.6657	52.4	L6	mus.	he	0.4123	55.1	L6	mus.	kf
	0.6494	57.1	L6	mus.	hf/ke	0.4099	33.1	L7	mus.	te/af
	0.6233	89.1	L6	mus.	hf/ke	0.3491	60.1	L6	mus.	hf

The abbreviations used are: muscle (mus.), cutaneous (cut.), hip (h), knee (k), ankle (a), flexion (f), extension (e), anterior (ant.), lateral (lat.) and med. (medial).

position because of the biomechanical linkage between joints (Bosco & Poppele, 2001).

How well does the linear decoder derived from one type of movement predict movements of a different type? In other words, is it a general model for a wide range of movements or only useful for the particular movements used to derive it? To answer these questions, we used data from pseudorandom movements as the training set (40 units, see Fig. 9*A*) and tested our predictions on walking-like (Fig. 9*B*) and centre-out movements (Fig. 9*C*). The centre-out task is a commonly used model in which movements are made from a central point to a number of positions around the periphery. In each part of the figure, the predicted distance and orientation (dots) fitted the actual data well (continuous lines), as indicated by the VAF and r.m.s. error. From the values in polar coordinates, the movement in the sagittal plane was again calculated and the predicted and actual trajectories are shown. The r.m.s. errors of the predictions from the actual positions were 1.1 cm (random), 1.7 cm (walking-like movements) and 2.3 cm (centre-out movements).

The poorest fit was to the centre-out movements, but the accuracy of the fit is hard to appreciate visually in the right-hand panel of Fig. 9*C*, because centre-out movements were somewhat irregular when produced manually. In another experiment a robot produced more reliable centre-out movements. These are shown in Fig. 10, together with the fits for a training set and a test set. The VAF and r.m.s. error were 98% and 0.7 cm, respectively, for the training set and 91% and 1.6 cm, respectively, for the test set. These fits were also produced using a slightly different method that will be described in relation to a muscle-based model in the Appendix.

Discussion

This study examines the coding of global, whole-limb information by populations of first-order afferents during continuous, time-varying movements. The analysis was done in two stages. First, we used a simple linear regression to describe how position and velocity information is encoded by the firing rate of a neurone. Then, the process was reversed to study how the firing rates of the neurones could be decoded to predict the position and velocity of the limb. While previous related work focused on how a homogeneous population of afferents encodes specific kinematic inputs and force (Prochazka & Gorassini, 1998*a*; Jones *et al.* 2001; Cordo *et al.* 2002; Ribot-Ciscar *et al.* 2003), we focused both on encoding in individual neurones and on predicting time-varying kinematic variables from the firing rates (decoding). This

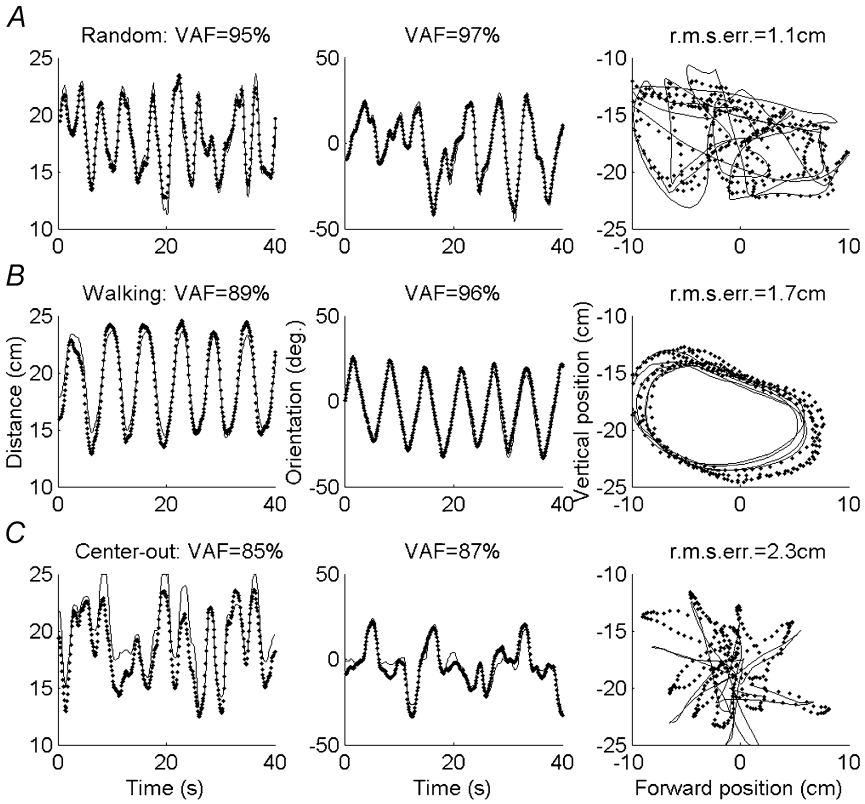

Figure 9. Data from a random trial were used to predict the distance and orientation of the toe with respect to the hip in the same trial (*A*), and in trials where the limb was moved in a walking-like pattern (*B*) or from a central position to a variety of outer targets (*C*)
The VAF is shown for each variable as well as the predicted (dots) and the actual positions (continuous lines).

approach led to several important insights that were not obvious from previous studies that recorded serially from sensory neurones (e.g. see the review by Prochazka, 1996).

First, we found that decoding based on the activity of a selected subset containing less than 10 cells may provide an accurate representation of the position of the limb in the sagittal plane. Second, we have shown that these representations generalize across different kinds of movements (i.e. from pseudorandom to walking-like and centre-out movements). Third, our analysis provides a method of assessing the contribution of different receptor types to limb position coding. Muscle receptors contributed most to the determination of the limb position. Cutaneous afferents, particularly in skin overlying joints, were also important. Joint afferents may be involved, but many joint afferents are only active at the extremes of motion that were not explored fully. Under the passive, anaesthetized conditions studied, Golgi tendon organs are relatively difficult to activate and may be hard to distinguish from joint afferents since the tendon organs are very insensitive in an anaesthetized preparation.

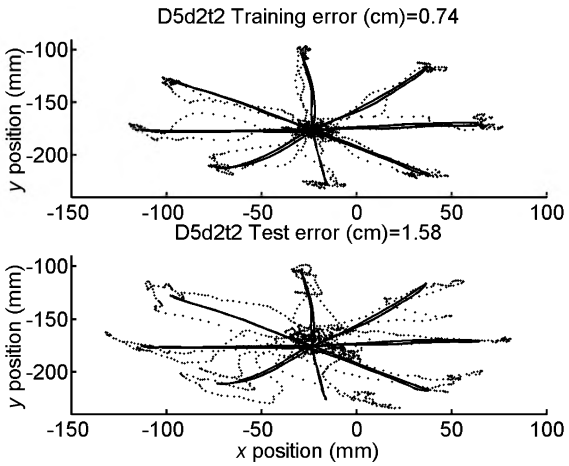

Figure 10. Predicted position (dots) for centre-out movements produced by the robotic manipulator (continuous lines)
The first set of movements was used to determine the linear regression coefficients (training) and these coefficients were used to predict the second set of movements. The r.m.s. error is given using a joint angle coordinate system with 50 units and a time constant of 200 ms.

Before discussing the nature of the coding process and its functional implications for the control of movement, several points should be stated. First, although even a few neurones can predict limb position accurately, this does not mean that recordings from only a few cells are needed or that the nervous system only uses a few cells. The cells that gave the optimal predictions in the test set were selected from the recorded neurones that were best correlated to the kinematics in the training set. Selecting much larger numbers at random did not give as good a prediction (our unpublished observations). Without having access to a substantial population of cells simultaneously, this result would probably not have emerged. Numerous previous studies, reviewed by

Prochazka (1996), have recorded serially from sensory neurones in the leg, with a wide range of kinematic profiles (e.g. the locomotor step cycle) without exploring the possibility of predicting global variables such as the position of the toes in space. The deterioration of 'test' generalization as a result of including all neurones is a new finding, as well as the resulting suggestion that neural decoding studies should rely on a small number of selected neurones. Selecting a limited number of optimal neurones has not been tried in other systems, such as the motor cortex. If a similar result emerges, the number of cortical neurones needed for a reliable multiunit decoder (Wessberg *et al.* 2000; Nicolelis, 2003) may have been greatly over-estimated.

Second, our results do not necessarily imply that the somatosensory system has great redundancy. Large numbers of neurones are clearly needed to sense the precise location of a stimulus applied to a point on the leg or to discriminate between two closely spaced points. Neurones involved in these fine discriminations may contribute little or nothing to the global sense of limb position.

Third, the results may be different during normal behaviour. Varying fusimotor inputs will influence the discharge of the muscle spindles (Matthews, 1972; Prochazka, 1989). Cutaneous receptors, particularly from the skin of the paw, will fire in response to ground reaction forces and other forces that are applied to the paw during normal activities. Golgi tendon organs will be much more active during muscle contractions. Nonetheless, similar methods have been successful in relation to limb position in decerebrate animals and in animals walking freely on a treadmill (Weber *et al.* 2002; Poppele *et al.* 2003). Ensemble recordings in animals and recent human work suggest that muscle spindles basically function as stretch receptors, even during voluntary movements that include fusimotor activity (Prochazka & Gorassini, 1998*b*; Jones *et al.* 2001). Thus, these studies under anaesthesia are a good starting point for understanding coding in the freely moving animal. Finally, we have used a number of automated processing steps to extract and edit the spike trains from up to 100 electrodes. A detailed justification of the methods has been presented elsewhere (Shoham *et al.* 2003; Stein & Weber, 2004; Stein *et al.* 2004) and will not be discussed further here.

Processing of the data in relation to sensory function

The firing rate of muscle receptors is linearly related to muscle length and velocity within a limited range (Terzuolo & Washizu, 1962; Matthews & Stein, 1969). Some have argued that the relationship to velocity is better described by a power function with an exponent less than 1, rather than a linear relationship (Houk *et al.* 1981; Prochazka & Gorassini, 1998*a*). However, a linear relationship is a good first approximation, and including velocity to a fractional power did not improve the fit

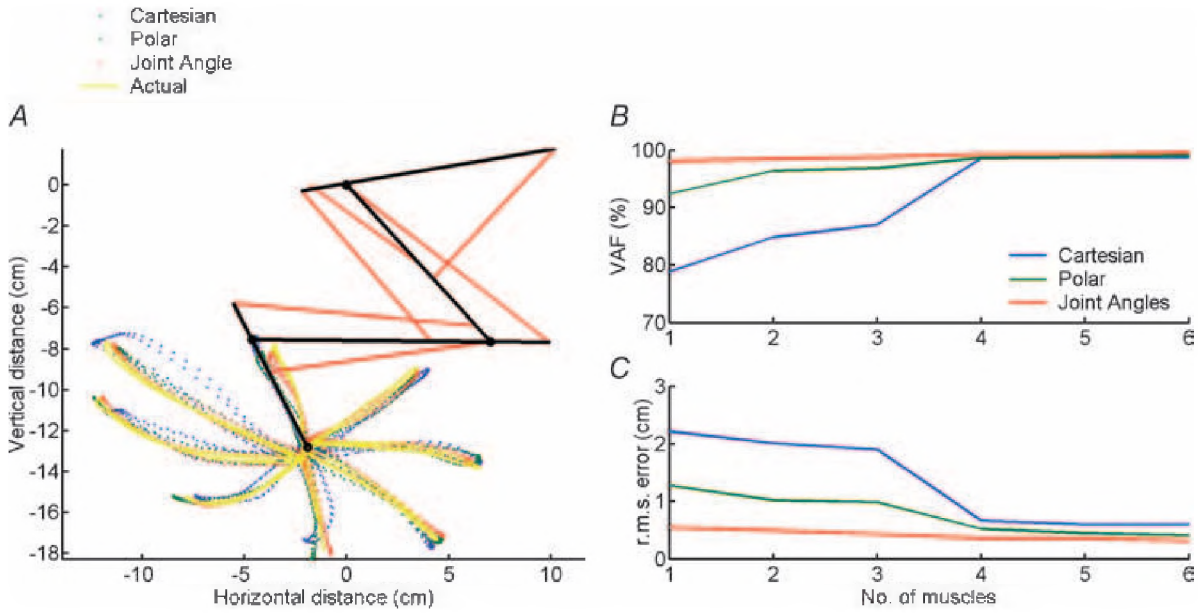

Figure 11. A model containing 6 muscle groups (red lines in *A*) was used (see Appendix and Discussion) to test how well muscle receptors could predict toe position
The muscle groups are hip flexors, hip extensors, bi-articular knee flexor/hip extensors, knee extensors, ankle flexors and ankle extensors. The trajectory produced by the robot in the centre-out task (yellow line) was compared with the predictions from receptors in 6 muscles (dots) in Cartesian (blue), polar (green) or joint angles (red). A high VAF (*B*) and a low r.m.s. error (*C*) are observed with as few as 4 receptors. The best fit was with joint angles and the worst fit with Cartesian coordinates.

significantly (our unpublished observations). Inclusion of acceleration terms did not lead to a statistically significant improvement in fitting the population of cells studied (Fig. 4). Cutaneous receptors have usually been studied in relation to precise stimuli applied to their receptive fields, rather than movements of a whole limb (Burke *et al.* 1988; Johnson, 2001). For consistency, the same processing was employed here to all units.

In addition, the spike rates were filtered with a second-order, critically damped, low-pass filter. This particular filter was chosen because its impulse response is a waveform that has often been fitted to EPSPs (Jack *et al.* 1975). The only free parameter is the rate constant that was optimal in the range of 15–30 rad s^{-1}, which corresponds to a time constant of 33–67 ms. The appropriate rate constants for EPSPs in various pathways that receive inputs from primary sensory neurones are not known. Similar results were obtained with shorter time constants, but the VAF was somewhat reduced.

The linear decoding methods gave remarkably good predictions of the position and velocity of the toe in space. Such predictions have rarely been attempted because of the limitations of single-unit recording methods. The best attempt in the somatosensory system is the work of Bosco and Poppele (Bosco & Poppele, 2001, 2003; Poppele *et al.* 2001). Our study extended this work to a variety of continuous movements and demonstrated good predictions using only a few, selected neurones. Though our results only show that linear algebraic methods can predict limb kinematics, analogous methods in the nervous system are quite plausible. The linear weighting of the synaptic action of different neurones could be genetically 'hard-wired' and/or learnt by trial and error. In this way the sense of limb position we perceive would be matched to the knowledge of where our limbs are in space, derived from other sensory modalities such as vision.

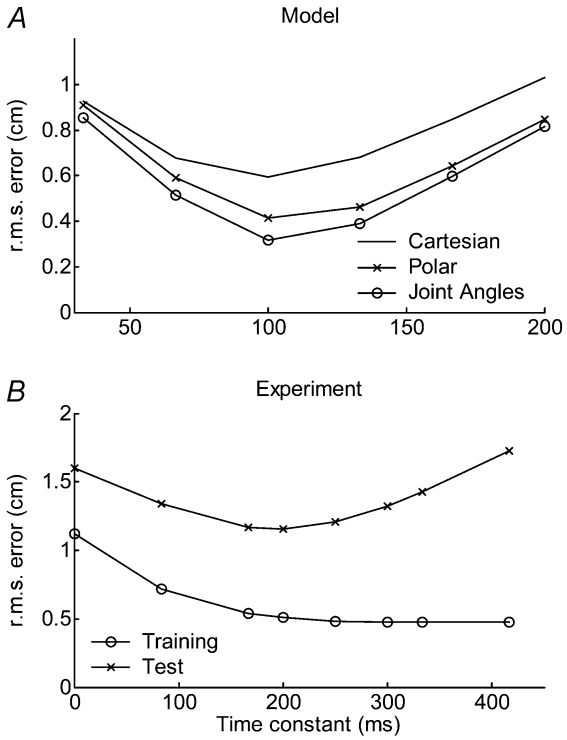

Figure 12. The effect of the time constant on the r.m.s. error in the model of Fig. 11 (*A*) and in the experiment shown in Fig. 10 (*B*)

The time constant used in the model was 100 ms and this value gave the best fit, as expected. In the training set of Fig. 10 a longer time constant produced a better fit to the experimental data. However, in the test set, there was a clear, best fit with a value near 200 ms.

How can sensory neurones predict global variables such as toe position?

Positions and velocities were initially predicted independently, but the two are obviously combined in the firing rate. If the firing rate, $f(t)$, is a linear sum of position terms and velocity terms:

$$f(t) = a + bx(t) + c(\mathrm{d}x/\mathrm{d}t), \tag{7}$$

where a is the offset (firing rate in spikes s^{-1}, when $x(t)$ and $\mathrm{d}x/\mathrm{d}t$ are 0); and b and c are factors converting from units of position (m) and velocity (m s^{-1}) to units of firing rate (spikes s^{-1}). Then, position can be predicted by solving eqn (7) for $x(t)$. The result is:

$$x(t) = \frac{1}{c}\int_0^t f(t-\tau)\exp(-b\tau/c)\mathrm{d}\tau, \tag{8}$$

For simplicity the initial conditions have been ignored in eqn (8). The ratio c/b is a time constant (s) in the convolution integral of eqn (8) and should not be confused with the filter time constant mentioned in the Methods. Also, there are a number of position and velocity variables, of which $x(t)$ and $\mathrm{d}x/\mathrm{d}t$ are simply examples in Cartesian coordinates. Finally, the firing rates of many neurones contribute to the determination of toe position, so $f(t)$ will be a weighted sum of the firing rates of each neurone. Figure 10 was determined using eqn (8) with 50 neurones.

Figure 11 uses a model described in the Appendix, containing a few muscles with muscle receptors that obey eqn (7), where $x(t)$ is now the length of the muscle. This figure also shows that muscle receptors in just a few muscles can give a good prediction of the position of the toe in space, using eqn (8). Figure 12 examines the temporal aspects of the same model. In the model we arbitrarily used a time constant of 100 ms, and Fig. 12*A* shows, as expected, that the least error occurs when a time constant of 100 ms is used in the calculations. In the biological system, selecting a time constant of 200 ms gave the most accurate predictions. In other words, to predict toe position optimally, a 'leaky integrator' with a time constant of

200 ms is required. Further work might test whether spinocerebellar cells, for example, provide the optimal time constant to predict limb position to the cerebellum and other higher structures.

Overall, the predictions of position had an accuracy of 1–2 cm (Figs 7, 9 and 10). Recording from more cells may further improve the predictions, but we are not aware of any psychophysical data on the absolute accuracy of limb position sense in the sagittal plane for humans, much less for cats. What has been measured experimentally is the amount a joint must be moved at a certain velocity before a subject can detect it. For example, movements of the human hip, knee and ankle by about 1 deg can be detected (Refshauge *et al.* 1995). If the sensitivity is the same in the cat and the movements are scaled to a leg length of about 25 cm, then a 1 deg movement of the hip would move the toe 0.43 cm. Further studies are needed to measure the accuracy with which a subject can specify the position of the toe or hand in space, rather than detection thresholds when the limb is moved. Work over the last 20 years has suggested that the motor cortex plans movements in terms of distances and directions, essentially a polar coordinate system (Georgopoulos *et al.* 1982; Schwartz, 1994; Serruya *et al.* 2002; but see Scott *et al.* 2001 for a different interpretation). This paper shows how sensory receptors can provide appropriate information to guide such movements.

Appendix

Figure 11*A* shows a simplified model of the muscles of the hindlimb of the cat, which was used to determine if a few muscle receptors can predict the position of an end-point. Six muscles are shown as red lines connecting different limb segments, based on the model of Yakovenko *et al.* (2004), which in turn was derived from Goslow *et al.* (1973). The continuous yellow lines give the movements of the cat's paw in the centre-out task. The different coloured dots show the predicted movements from the responses of simulated muscle receptors. The firing rates of the simulated receptors were given by a sum of length and velocity contributions of each muscle, as given by eqn (8). The lengths and velocities were calculated from the experimentally measured joint positions and angles. The predicted end-point was calculated from eqn (8) with a time constant of 100 ms. Predicted positions deviate from the actual positions more in Fig. 11*A* for Cartesian coordinates than for the polar or joint angular coordinates, as found experimentally (Stein *et al.* 2004). Furthermore, as few as four receptors are needed to produce a high VAF (Fig. 11*B*) or a low r.m.s. error (Fig. 11*C*). The errors are smaller than found experimentally because no non-linearities or sources of variability were included in the model.

Figure 12 gives one final example of interest. In Fig. 12*A* the r.m.s. error for the model is shown in the three coordinate systems as a function of the time constant. The minimum error occurs for a time constant of 100 ms in all coordinate systems. This result shows the self-consistency of the model, since 100 ms was the value used in the model. Figure 12*B* shows the same calculation for the experimental data. There is again a clear minimum, but experimentally the minimum occurs with a time constant near 200 ms. The predictions of Fig. 10 used this time constant.

References

Aoyagi Y, Stein RB, Branner A, Pearson KG & Normann RA (2003). Capabilities of a penetrating microelectrode array for recording single units in dorsal root ganglia of the cat. *J Neurosci Meth* **128**, 9–20.

Bialek W, Rieke F, de Ruyter van Steveninck RR & Warland D (1991). Reading a neural code. *Science* **252**, 1854–1857.

Bosco G & Poppele RE (2001). Proprioception from a spinocerebellar perspective. *Physiol Rev* **81**, 539–568.

Bosco G & Poppele RE (2003). Modulation of dorsal spinocerebellar responses to limb movement. II. Effect of sensory input. *J Neurophysiol* **90**, 3372–3382.

Burke D, Gandevia SC & Macefield G (1988). Responses to passive movement of receptors in joint, skin and muscle of the human hand. *J Physiol* **402**, 347–361.

Collins DF, Refshauge KM & Gandevia SC (2000). Sensory integration in the perception of movements at the human metacarpophalangeal joint. *J Physiol* **529**, 505–515.

Cordo PJ, Flores-Vieira C, Verschueren SM, Inglis JT & Gurfinkel V (2002). Position sensitivity of human muscle spindles: single afferent and population representations. *J Neurophysiol* **87**, 1186–1195.

Gandevia SC, Hall LA, McCloskey DI & Potter EK (1983). Proprioceptive sensation at the terminal joint of the middle finger. *J Physiol* **335**, 507–517.

Gandevia SC, Refshauge KM & Collins DF (2002). Proprioception: peripheral inputs and perceptual interactions. *Adv Exp Med Biol* **508**, 61–68.

Georgopoulos AP, Kalaska JF, Caminiti R & Massey JT (1982). On the relations between the direction of two-dimensional arm movements and cell discharge in primate motor cortex. *J Neurosci* **2**, 1527–1537.

Goslow GE, Reinking RM & Stuart DG (1973). The cat step cycle: hind limb joint angles and muscle lengths during unrestrained locomotion. *J Morph* **141**, 1–42.

Guillory KS & Normann RA (1999). A 100-channel system for real time detection and storage of extracellular waveforms. *J Neurosci Meth* **91**, 21–29.

Houk JC, Rymer WZ & Crago PE (1981). Dependence of dynamic response of spindle receptors on muscle length and velocity. *J Neurophysiol* **46**, 143–166.

Jack JJB, Noble D & Tsien RW (1975). *Electric Current Flow in Excitable Cells*. Clarendon Press, Oxford.

Johnson KO (2001). The roles and functions of cutaneous mechanoreceptors. *Curr Opin Neurobiol* **11**, 455–461.

Jones KE, Wessberg J & Vallbo AB (2001). Directional tuning of human forearm muscle afferents during voluntary wrist movements. *J Physiol* **536**, 635–647.

Loeb GE, Hoffer JA & Pratt CA (1985). Activity of spindle afferents from cat anterior thigh muscles. I. Identification and patterns during normal locomotion. *J Neurophysiol* **54**, 549–564.

McCloskey DI, Cross MJ, Honner R & Potter EK (1983). Sensory effects of pulling or vibrating exposed tendons in man. *Brain* **106**, 21–37.

Macefield G, Gandevia SC & Burke D (1990). Perceptual responses to microstimulation of single afferents innervating joints, muscles and skin of the human hand. *J Physiol* **429**, 113–129.

Matthews PBC (1972). *Mammalian Muscle Receptors and Their Central Actions*. Arnold, London.

Matthews PBC & Stein RB (1969). The sensitivity of muscle spindle afferents to small sinusoidal changes in length. *J Physiol* **200**, 723–743.

Mountcastle VB (1980). Central nervous mechanisms in sensation. In *Medical Physiology*, 14th edn, ed. Mountcastle VB, pp. 327–427. Mosby, St Louis.

Nicolelis MA (2003). Brain–machine interfaces to restore motor function and probe neural circuits. *Nature Rev Neurosci* **4**, 417–422.

Poppele RE, Bosco G & Rankin AM (2001). Independent representations of limb axis length and orientation in spinocerebellar response components. *J Neurophysiol* **87**, 409–422.

Poppele RE, Rankin A & Eian J (2003). Dorsal spinocerebellar tract neurons respond to contralateral limb stepping. *Exp Brain Res* **149**, 361–370.

Prochazka A (1989). Sensorimotor gain control: a basic strategy of motor systems? *Progr Neurobiol* **33**, 281–307.

Prochazka A (1996). Proprioceptive feedback and movement regulation. In *Handbook of Physiology, section 12, Exercise: Regulation and Integration of Multiple Systems*, ed. Rowell L & Sheperd JT, pp. 89–127. Oxford University Press, New York.

Prochazka A & Gorassini M (1998*a*). Models of ensemble firing of muscle spindle afferents recorded during normal locomotion in cats. *J Physiol* **507**, 277–291.

Prochazka A & Gorassini M (1998*b*). Ensemble firing of muscle spindle afferents recorded during normal locomotion in cats. *J Physiol* **507**, 293–304.

Refshauge KM, Chan R, Taylor JL & McCloskey DI (1995). Detection of movements imposed on human hip, knee, ankle and toe joints. *J Physiol* **488**, 231–241.

Ribot-Ciscar E, Bergenheim M, Albert F & Roll JP (2003). Proprioceptive population coding of limb position in humans. *Exp Brain Res* **149**, 512–519.

Richmond BJ, Optican LM, Podell M & Spitzer H (1987). Temporal encoding of two-dimensional patterns by single units in primate inferior temporal cortex. I. Response characteristics. *J Neurophysiol* **57**, 132–146.

Rousche PJ & Normann RA (1992). A method for pneumatically inserting an array of penetrating electrodes into cortical tissue. *Ann Biomed Eng* **20**, 413–422.

Salinas E & Abbott LF (1994). Vector reconstruction from firing rates. *J Comput Neurosci* **1**, 89–107.

Schwartz AB (1992). Motor cortical activity during drawing movements: single-unit activity during sinusoid tracing. *J Neurophysiol* **68**, 528–541.

Schwartz AB (1994). Direct cortical representation of drawing. *Science* **265**, 540–542.

Scott SH, Gribble PL, Graham KM & Cabel DW (2001). Dissociation between hand motion and population vectors from neural activity in motor cortex. *Nature* **413**, 161–165.

Serruya MD, Hatsopoulos NG, Paninski L, Fellows MR & Donoghue JP (2002). Instant neural control of a movement signal. *Nature* **416**, 141–142.

Sherrington CS (1906). *The Integrative Action of the Nervous System*. Yale University Press, New Haven, CT, USA.

Shoham S, Fellows MR & Normann RA (2003). Robust automatic spike sorting using mixtures of multivariate t-distributions. *J Neurosci Meth* **127**, 111–122.

Stein RB, Aoyagi Y, Weber DJ, Shoham S & Normann RA (2004). Encoding mechanisms for sensory neurons studied with a multielectrode array in the cat dorsal root ganglion. *Can J Physiol Pharmacol* (in press).

Stein RB & Weber DJ (2004). Editing trains of action potentials from multi-electrode arrays. *J Neurosci Meth* **134**, 91–100.

Taylor DM, Helms Tillery SI & Schwartz AB (2002). Direct cortical control of 3D neuroprosthetic devices. *Science* **296**, 1829–1832.

Terzuolo CA & Washizu Y (1962). Relation between stimulus strength, generator potential and impulse frequency in stretch receptor of crustacea. *J Neurophysiol* **25**, 56–66.

Weber DJ, Stein RB, Aoyagi Y & Normann RA (2002). Chronic multi-unit recording of sensory neuronal activity in the cat dorsal root ganglion. *Soc Neurosci Abstract* 348.7.

Wessberg J, Stambaugh CR, Kralik JD, Beck PD, Laubach M, Chapin JK *et al.* (2000). Real-time prediction of hand trajectory by ensembles of cortical neurons in primates. *Nature* **408**, 361–365.

Yakovenko S, Gritsenko V & Prochazka A (2004). Contribution of stretch reflexes to locomotor control: a modeling study. *Biol Cybern* **90**, 146–155.

Acknowledgements

This work was supported by grants to R.B.S. from the Canadian Institutes of Health Research and to R.A.N. from NIH. D.J.W. was a postdoctoral fellow supported by the Alberta Heritage Foundation for Medical Research and the Alberta Paraplegic Foundation.

Authors' present addresses

Y. Aoyagi: Department of Rehabilitation Medicine, Kawasaki Medical School, Okayama, Japan.

J. Wagenaar: Department of Biomedical Engineering, University of Twente, Enschede, the Netherlands.

S. Shoham: Department of Molecular Biology, Princeton, NJ, USA.